Thermal Band Observations of the May 2022 Total Lunar Eclipse by the Landsat Thermal Infrared Sensors

Matthew Montanaro[a], Dennis Reuter[a], Allen Lunsford[a], and James Briscoe[a]

[a]NASA Goddard Space Flight Center, 8800 Greenbelt Rd., Greenbelt, MD, USA 20771

ABSTRACT

The Thermal Infrared Sensor (TIRS) instruments on board Landsat 8 and Landsat 9 provide routine thermal band image measurements of the Earth for the Landsat program. Although these observatories are specifically designed for mapping the Earth's surface from their 705-km altitude orbits, they were recently utilized to image the Moon during the total lunar eclipse of May 2022. The full Moon is frequently used as a calibration target for Landsat. However, the imaging of the lunar eclipse provided a unique opportunity to gather accurate temporal thermal band data over the full lunar disc as solar illumination is removed. This campaign required a large effort by the Landsat Flight Operations teams to coordinate acquisitions and technical constraints on both observatories to capture the long temporal extent of the eclipse. The result of this effort was a series of resolved thermal images of the Moon at discrete times as the Earth's shadow swept across the lunar surface through the start, partial, and total phases of the eclipse. This sequence of images showed an overall drop in surface temperature from approximately 370 K to 180 K in about 300 minutes as solar insolation was removed. Furthermore, the spatial distribution of cooling rates from this unique event provided information about different material properties (density and thermal inertia) across the lunar surface and showed a clear distinction among mare, highlands, and impact craters.

Keywords: Landsat, TIRS, Thermal Infrared, Thermal Inertia, Moon, Lunar Eclipse

1. INTRODUCTION

Total lunar eclipses have spawned various myths and omens throughout history but can also provide an opportunity for modern scientific measurement. During this celestial alignment, the (full) Moon is opposite the Sun from Earth and passes through the Earth's shadow for a short time. To observers in visible light, the Moon appears to darken in the Earth's shadow as the illumination from the Sun is no longer directly reflected off its surface and back to the observer (Figure 1). At thermal infrared wavelengths, however, the Moon continues to radiate as a pseudo-blackbody due to the relatively warm temperatures of its surface materials. The infrared signature of the Moon has been studied from remote observations from Earth and lunar orbit and from in-situ measurements on the surface [1–3]. A total lunar eclipse, on the other hand, provides a unique opportunity to observe the temporal temperature change of the entire near-side of the Moon within a relative short (several-hour) time period.

The current generation of Landsat observatories carry highly accurate thermal band instruments that were recently called upon to image the total lunar eclipse in May 2022. Landsat 8 (L8) and Landsat 9 (L9) are near-identical observatories sharing the same 705-km altitude, 99-minute low Earth orbit and are spaced 180 degrees

Send correspondence to: matthew.montanaro@nasa.gov

Figure 1. Moon photographed at various times during the total lunar eclipse, 16 May 2022, with a Nikon D5600 DSLR camera, 600 mm lens, various exposure times and ISO settings, from Rochester, New York, USA by M. Montanaro.

apart so the same location on Earth is imaged by one of the observatories every eight days. The instrument payload on both spacecraft include the Thermal Infrared Sensor (TIRS) which acquires image data of the Earth in two long-wave infrared spectral channels (10.8 μm and 12.0 μm) [4, 5]. The instruments operate in a push-broom mode in which pixels from three detector arrays acquire image data at a 70 Hz frame rate with a ± 7.5 degree field of view. From this instrument and orbital configuration, the TIRS image swath is 185 km wide with a pixel resolution of 100 meters on the surface. The instruments are carefully calibrated to ensure radiometric uncertainties of less than 2% to enable derivation of land surface temperature products [6–8].

Although TIRS was designed for operational thermal band mapping of the Earth, a campaign to image the Moon at various times throughout the lunar eclipse was planned and executed in May 2022. Many technical, orbital, procedural, and planning factors needed to be considered when utilizing the observatories for these time-critical acquisitions. In the end, multiple thermal images were acquired by both TIRS instruments spanning the start, partial, and total phases of the eclipse. This article discusses the planning and execution of the eclipse scans, explains the image processing involved to produce temperature maps of the Moon, and presents the image results and how they contribute to the overall understanding of lunar materials.

2. IMAGING PLAN

The total lunar eclipse of 16 May 2022 occurred in several phases as the Moon's limbs entered and exited the penumbra and umbra portions of Earth's shadow. Since the Landsat observatories are in low Earth orbit, they could not be tasked to stare at the Moon and acquire continuous scans during the entirety of the eclipse. Specific times to scan the Moon needed to be selected well ahead of the event and, obviously, the selected times needed to coincide with occasions when each observatory had a direct line of sight to the Moon (i.e.- when on the night side of the orbit). Furthermore, exact commands for pointing and imaging needed to be created while considering operational constraints.

As mentioned previously, the Landsat spacecrafts and instruments are designed to image the Earth. They are operational assets, owned and operated by the US Geological Survey (USGS), that acquire over 700 individual Earth scenes per day that are released to users within hours of acquisition. The NASA-originated request to image the lunar eclipse could not significantly interfere with normal operations. In order to be acceptable, the proposed eclipse imaging sequence could not deviate considerably from established operational procedures with the on-orbit flight hardware. Fortuitously however, each observatory performs a special calibration activity once a month in which the full Moon is imaged by the instruments for calibration purposes. These lunar calibrations are primarily performed for the companion VNIR/SWIR instrument on Landsats 8 and 9 known as the Operational Land Imager (OLI), but TIRS also takes the opportunity to image the Moon for instrument trending purposes and to characterize optical stray light effects [9]. During this activity, on the night side of the orbit, the spacecraft is rotated from its normal Earth-pointing position and the instruments' fields of view are aimed at the Moon. The spacecraft then performs brief slews in the along-track direction as the instruments acquire image data in their push-broom mode. The spacecraft then slews back to the normal Earth-pointing attitude after the lunar scans are completed and Earth imaging resumes on the following daylight portion of the orbit. The intent of this calibration activity for TIRS is to image the Moon on each detector array twice. Due to the limited time on the night side of the orbit (approximately 30 minutes), the entire lunar calibration activity is divided into two consecutive orbits. For TIRS, on the night side of the first orbit, two scans of two detector arrays (four scans total) are acquired. On the night side of the next orbit, two scans of the remaining detector array are acquired. Thus each lunar calibration activity yields two scans per detector array for a total of six scans over two orbits.

Early in the planning process, the Flight Operations and Mission Planning teams concluded that the monthly lunar calibration activity could be utilized to perform the eclipse imaging. Doing so would use already established procedures and command sequences and save many hours of manual manipulation required to build and test a procedure from scratch. Given this path forward, several other items had to be considered before the imaging plan could be approved:

- Although the same lunar calibration command sequences would be used for the eclipse imaging, the time of execution would be different than a standard lunar calibration. Normally, this activity would be performed with lunar phase angles of around +5 to +9 degrees whereas the eclipse scans would take place at a phase

angle of 0 degrees. As such, flight controllers conducted a full simulation of the activity to uncover any interference on the field of view of the star trackers, solar impingement on the instrument field of view, radiator positioning, etc. before the activity was run on flight hardware.

- Each observatory would be unable to perform more than one lunar calibration activity per day due to how command tables are loaded and executed by the spacecraft. L9 would be able to execute another lunar calibration the day before the eclipse (15 May), but L8 cannot do the same due to limits on how it stores command tables.

- Other routine observatory activities (file clean up, telemetry downlink, etc.) that would normally occur during the night side of the orbit would need to be re-planned for different times. Additionally, any user-requested TIRS nighttime Earth imaging for the chosen orbits would have to sacrificed or moved to another orbit if possible.

- The Flight Operations teams had to consider the possibility that during the activity the observatory would detect a problem and put itself into a safe-hold state. Flight controllers had to be ready to recover the spacecraft and instruments in such an event. If one spacecraft entered a safe-hold condition, the eclipse sequence on the other spacecraft would be aborted to avoid the same situation.

- The imaging plan had to be approved by the Landsat Calibration and Validation team since their normal monthly lunar calibration acquisitions would be replaced with the eclipse scans.

- Coincidentally, L8 mission operations was planning to move from the legacy mission operations center (MOC) to a new combined L8/L9 MOC the same week as the lunar eclipse. Personnel were mostly occupied with moving (physically and electronically) assets from the legacy MOC to the new MOC which limited resources for planning the lunar eclipse activity.

Working within all constraints, the TIRS science team chose to target the beginning half of the eclipse. The full Moon would be imaged by L9 several hours before the start of the eclipse at the end of the previous day of year. L9 and L8 would then alternate scanning the Moon during the first partial phase and full phase of the eclipse. This arrangement would provide a good temporal sampling as the lunar surface cooled down with the removal of solar illumination. Table 1 lists the times of each TIRS image relative to the eclipse phases.

Day/Time	Event
15 May 2022 21:45*	L9 orbit 1, 2 detector arrays
15 May 2022 23:27*	L9 orbit 2, 1 detector array
16 May 2022 01:32:05	Penumbral Eclipse begins
16 May 2022 02:27:52	Partial Eclipse begins
16 May 2022 02:42*	L9 orbit 1, 2 detector arrays
16 May 2022 03:29:03	Full Eclipse begins
16 May 2022 03:32*	L8 orbit 1, 2 detector arrays
16 May 2022 04:11:28	Maximum Eclipse
16 May 2022 04:23*	L9 orbit 2, 1 detector array
16 May 2022 04:53:55	Full Eclipse ends
16 May 2022 05:13*	L8 orbit 2, 1 detector array
16 May 2022 05:55:07	Partial Eclipse ends
16 May 2022 06:50:49	Penumbral Eclipse ends

*approximate times, within +/-5 minutes of actual

Table 1. Times for the May 2022 lunar eclipse events along with the selected imaging opportunities for both Landsat 8 and Landsat 9 TIRS instruments. These imaging orbits were chosen based on orbital geometry and the desire to image the first half of the total eclipse (full Moon through full eclipse).

Both Landsat observatories successfully executed all planned lunar eclipse imaging activities and recorded the expected image data files and then returned to nominal Earth imaging. All image files were successfully downlinked on subsequent orbits.

3. IMAGE PROCESSING

All aspects of the TIRS instrument architecture and calibration were designed for Earth imagery collection and not for lunar imaging. The images acquired during the lunar eclipse scans therefore required custom image processing steps to account for several non-standard acquisition factors. On the geometry side, the TIRS frame rate is fixed to provide ideal sampling of the Earth's surface in the push-broom image collection mode from its low Earth orbit (i.e.- minimal over- and under-sampling in the along-track direction). During the lunar scans, the spacecraft slews (rotates) in the along-track direction as the instrument acquires push-broom image data. This slew rate is slower than the typical Earth orbit rate and resulted in images that were over-sampled by 8.4x in the along-track direction. On the radiometry side, TIRS is required to image without saturating between source temperatures of 240 K to 360 K to accommodate typical Earth temperatures over the seasons. Since the Moon has an effective temperature of almost 400 K in daylight, the integration time was lowered to prevent saturation of the detectors. When converting raw detector counts to radiance units, the established calibration functions, which are only defined for a 200 K to 360 K source range, were extrapolated for the Moon's warmer temperatures in daylight and cooler temperatures in shadow.

The image processing procedure, illustrated in Figure 2, involved applying radiometric and geometric steps to convert raw pixel data into the final temperature image. The raw data was linearized per the standard TIRS processing functions (see reference [10]) and then multiplied by the ratio of the standard integration time for Earth imagery to the integration time used for the lunar scans. The digital counts were now within the necessary range for the radiometric calibration functions. A portion of the image where deep space was imaged (several lunar diameters away from the Moon) was used as a background baseline to subtract from the lunar image. This subtracted image was then converted to radiance through the standard calibration functions for

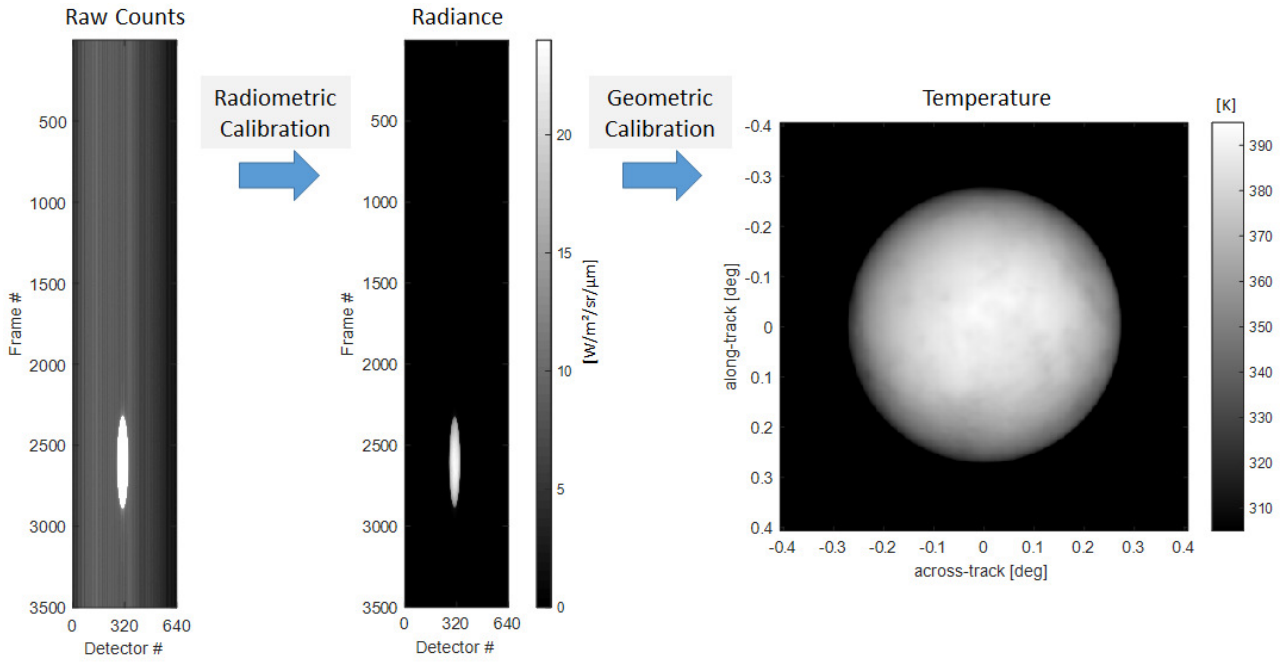

Figure 2. Illustration of the image processing steps to convert the raw lunar scan image from one detector array (left) into spectral radiance units (center) through the radiometric calibration process followed by a geometric calibration and conversion to brightness temperature (right). All final images have been rotated to the same orientation and upsampled by 4x4 to smooth the pixelation. Images contrasts are stretched to reveal variations over the lunar disc.

each detector. The resulting pixel values were in units of spectral radiance $[W/m^2/sr/\mu m]$ with uncertainties of less than 2% between source temperatures of 200 K to 360 K, and with slightly higher uncertainties outside that source range due to extrapolation of the calibration functions. Finally, the pixel radiances were converted to brightness temperatures assuming an emissivity of one.

A geometric resampling was performed next to account for the oversampling in the along-track direction. Spacecraft pointing telemetry (quaterions) for each image line along with Earth and Moon ephemeris data were used to calculate line-of-sight pointing for each image pixel. These pointing vectors were then resampled to a uniform pixel grid to create a rectified Moon image with a resolution of approximately 50 km/pixel on the Moon. Since each lunar scan was acquired from a different angle relative to the Moon's axis, each image was rotated to the same orientation to allow for temporal analysis of each pixel. A final 4x4 upsampling was performed on each image to smooth out the pixelation artifacts.

4. RESULTS

All lunar image data were processed in the same way and to the same temperature units, and final calibrations between L8 and L9 were verified to be consistent with each other. The resulting dataset covers the full spatial extent of the Moon at discrete time samples spanning the entire first half of the eclipse through totality. A total of twelve image files were acquired by L9 and six image files by L8. Of these, seven images were selected with the greatest separation in time among them (i.e. - an image that was acquired within several minutes of another image was not selected). The final dataset is displayed chronologically in Figure 3. For presentation purposes, only images from the TIRS 12.0 μm spectral channel are displayed here but images from the 10.8 μm channel are very similar. The contrast scale for each individual image is adjusted according to the minimum and maximum temperature of the lunar disc in the image and this temperature range is labeled for each image along with the time of acquisition. Brighter pixels represent warmer temperatures than darker pixels.

The temporal temperature dataset acquired during the total lunar eclipse offers a unique view of the Moon. In full solar illumination, the temperature distribution across the lunar surface varies roughly between 300 K and 400 K. Surface temperatures drop very quickly, greater than 100 K/hr, once solar insolation is removed. In full eclipse, the Moon's surface temperature ranges between roughly 160 K and 200 K. The rapid temperature decline is attributed to the properties of the lunar regolith. This fine-grain, low-density material has a relatively low thermal inertia and therefore tends to reach thermal equilibrium with the environment quickly. The lack of a dense atmosphere around the Moon also plays a factor in the rapid heat loss by the surface. Close examination of the thermal images reveals a small distinction between the lunar highland material (slightly cooler) and the lunar mare regions (slightly warmer), again attributed to differences in the thermal inertia and emissivity properties of the materials.

The larger thermal anomalies observed in the fully eclipsed images correspond to impact craters, with Tycho crater in the southern hemisphere as the most prominent region. The temporal dataset is useful in examining the thermal evolution of Tycho relative to its immediate surrounding material as shown in Figure 4. A temperature graph of the two regions illustrates the different cooling rates and thermal properties of the two materials. The crater's temperature lags the surrounding region's temperature when in full Sun by about 10 K. However, when

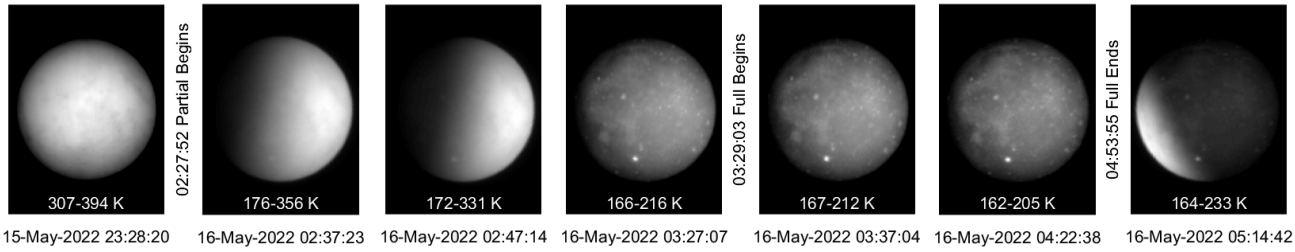

Figure 3. Selected TIRS thermal images (12.0 μm) spanning the total lunar eclipse from the full, un-eclipsed Moon through and past the full eclipsed phase from left to right. Each image is labeled with the acquisition time and the range of temperatures over the lunar disc and each image is contrast-scaled to this temperature range. The lunar north pole is straight up in the images.

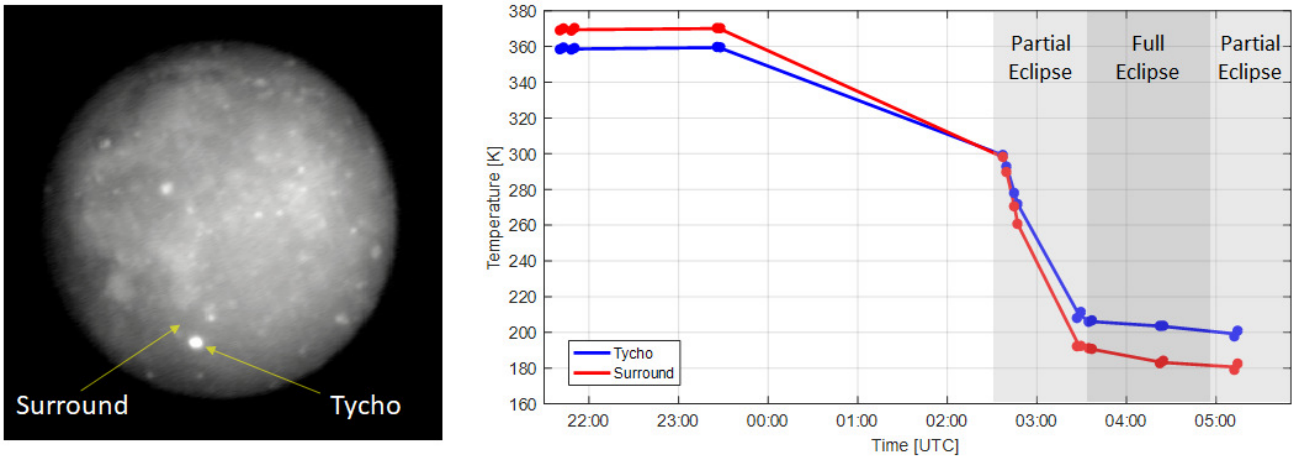

Figure 4. Moon imaged at full eclipse (16 May 2022, 04:22:38 UTC) demonstrates the higher temperatures (brighter pixels) retained by impact craters with the most prominent area, Tycho crater, labeled (left). Observations of Tycho relative to the immediate surrounding area throughout the eclipse reveals a thermal differential between the two material types (right).

sunlight is removed, the crater retains heat longer and is about 20 K warmer than the surrounding region after approximately 150 minutes. This observation is again explained by the higher density and higher thermal inertia of the crater due to its compacted material. The lower density of the surrounding region allows this material to release heat more efficiently. These results are consistent with long term measurements from lunar orbit by the Lunar Reconnaissance Orbiter (LRO) Diviner instrument which derived global thermal inertia maps from surface temperature image data [11–13]. Whereas assets in lunar orbit build up their measurements of the surface over many years, these TIRS measurements capture the entire near-side of the Moon in only a few measurements over a few hours and serve as a verification of the orbiter datasets.

5. SUMMARY

The Thermal Infrared Sensors aboard Landsat 8 and Landsat 9 were redirected from their routine thermal mapping of the Earth to image the total lunar eclipse in May 2022. Flight controllers managed to plan around a number of constraints to acquire image data at various times during the first half of the eclipse from the start and through totality. Custom image processing of the resulting data files were necessary to account for the non-standard (i.e.- non-Earth) image acquisitions. Although lunar material undergoes a thermal cycle every month, the total lunar eclipse offered a unique opportunity to observe thermal rates over the entire lunar near-side within a compressed timescale of several hours. The TIRS instruments observed a rapid temperature decline across the lunar surface as soon as direct solar illumination was removed. Variations in cooling rates revealed differences in the thermal inertia of surface materials, with high-density and high-inertia materials retaining heat longer than lower-density materials. The effect is especially notable for impact craters which exhibited much higher temperatures relative to the surrounding areas when in full shadow. The spatial and temporal results of this eclipse imaging opportunity has demonstrated how orbiting Earth science assets, with some modifications, may be utilized to perform cross-disciplinary science and serve as another tool for the space science community.

ACKNOWLEDGMENTS

The success of the eclipse imaging campaign was due to the dedication and support of the Landsat Flight Operations and Mission Planning teams, especially Jenn Rech, Jen White, Patrick Morinelli, Matt Fatig, Patty Molina, Sara Walmach, Cierra Slade, and Sophia LoSchiavo, who worked tirelessly to plan out all details of the intricate spacecraft maneuvers and image acquisitions.

REFERENCES

[1] Pugh, M. J. and Bastin, J. A., "Infrared observations of the moon and their interpretation," *The Moon* **5**, 16–30 (1972).

[2] Chin, G., Brylow, S., Foote, M., Garvin, J., Kasper, J., Keller, J., Litvak, M., Mitrofanov, I., Paige, D., Raney, K., Robinson, M., Sanin, A., Smith, D., Spence, H., Spudis, P., Stern, S. A., and Zuber, M., "Lunar Reconnaissance Orbiter overview: The instrument suite and mission," *Space Science Reviews* **129**, 391–419 (2017).

[3] Langseth, M. G., Clark, S. P., Chute, J. L., Keihm, S. J., and Wechsler, A. E., "The Apollo 15 lunar heat-flow measurement," *The Moon* **4**, 390–410 (1972).

[4] Reuter, D., Richardson, C., Pellerano, F., Irons, J., Allen, R., Anderson, M., Jhabvala, M., Lunsford, A., Montanaro, M., Smith, R., Tesfaye, Z., and Thome, K., "The Thermal Infrared Sensor (TIRS) on Landsat 8: Design overview and pre-launch characterization," *Remote Sensing* **7**(1), 1135–1153 (2015).

[5] Hair, J. H., Reuter, D. C., Tonn, S. L., McCorkel, J., Simon, A. A., Djam, M., Alexander, D., Ballou, K., Barclay, R., Coulter, P., Edick, M., Efremova, B., Finneran, P., Florez, J., Graham, S., Harbert, K., Hewitt, D., Hickey, M., Hicks, S., Hoge, W., Jhabvala, M., Lilly, C., Lunsford, A., Mann, L., Masters, C., Montanaro, M., Muench, T., Otero, V., Parong, F., Pearlman, A., Penn, J., Vigneau, D., and Wenny, B., "Landsat 9 Thermal Infrared Sensor 2 architecture and design," in [*2018 IEEE International Geoscience and Remote Sensing Symposium (IGARSS)*], 8841–8844 (2018).

[6] Gerace, A. and Montanaro, M., "Derivation and validation of the stray light correction algorithm for the Thermal Infrared Sensor onboard Landsat 8," *Remote Sensing of Environment* **191**, 246–257 (2017).

[7] Pearlman, A., Efremova, B., Montanaro, M., Lunsford, A., Reuter, D., and McCorkel, J., "Landsat Thermal Infrared Sensor 2 on-orbit calibration and initial performance," *IEEE Transactions on Geoscience and Remote Sensing* **60**(1002608), 1–8 (2022).

[8] Gerace, A., Kleynhans, T., Eon, R., and Montanaro, M., "Towards an operational, split window-derived surface temperature product for the Thermal Infrared Sensors onboard Landsat 8 and 9," *Remote Sensing* **12**(2), 224 (2020).

[9] Montanaro, M., McCorkel, J., Tveekrem, J., Stauder, J., Mentzell, E., Lunsford, A., Hair, J., and Reuter, D., "Landsat Thermal Infrared Sensor 2 stray light mitigation and assessment," *IEEE Transactions on Geoscience and Remote Sensing* **60**(5002408), 1–8 (2022).

[10] Pearlman, A., Montanaro, M., Efremova, B., McCorkel, J., Wenny, B., Lunsford, A., and Reuter, D., "Prelaunch radiometric calibration and uncertainty analysis of Landsat Thermal Infrared Sensor 2," *IEEE Transactions on Geoscience and Remote Sensing* **59**(4), 2715–2726 (2021).

[11] Hayne, P. O., Bandfield, J. L., Siegler, M. A., Vasavada, A. R., Ghent, R. R., Williams, J.-P., Greenhagen, B. T., Aharonson, O., Elder, C. M., Lucey, P. G., and Paige, D. A., "Global regolith thermophysical properties of the moon from the Diviner Lunar Radiometer Experiment," *Journal of Geophysical Research* **122**(12), 2371–2400 (2017).

[12] Williams, J.-P., Paige, D., Greenhagen, B., and Sefton-Nash, E., "The global surface temperatures of the moon as measured by the Diviner Lunar Radiometer Experiment," *Icarus* **283**, 300–325 (2017).

[13] Vasavada, A. R., Bandfield, J. L., Greenhagen, B. T., Hayne, P. O., Siegler, M. A., Williams, J.-P., and Paige, D. A., "Lunar equatorial surface temperatures and regolith properties from the Diviner Lunar Radiometer Experiment," *Journal of Geophysical Research* **117** (2012).